World Academy of Science, Engineering and Technology
International Journal of Mechanical and Mechatronics Engineering
Vol:2, No:5, 2008

Numerical Investigation of Delamination in Carbon-Epoxy Composite using Arcan Specimen

M. Nikbakht, and N. Choupani

***Abstract*—**In this paper delamination phenomenon in Carbon-Epoxy laminated composite material is investigated numerically. Arcan apparatus and specimen is modeled in ABAQUS finite element software for different loading conditions and crack geometries. The influence of variation of crack geometry on interlaminar fracture stress intensity factor and energy release rate for various mixed mode ratios and pure mode I and II was studied. Also, correction factors for this specimen for different crack length ratios were calculated. The finite element results indicate that for loading angles close to pure mode-II loading, a high ratio of mode-II to mode-I fracture is dominant and there is an opposite trend for loading angles close to pure mode-I loading. It confirms that by varying the loading angle of Arcan specimen pure mode-I, pure mode-II and a wide range of mixed-mode loading conditions can be created and tested. Also, numerical results confirm that the increase of the mode-II loading contribution leads to an increase of fracture resistance in the CF/PEI composite (i.e., a reduction in the total strain energy release rate) and the increase of the crack length leads to a reduction of interlaminar fracture resistance in the CF/PEI composite (i.e., an increase in the total interlaminar strain energy release rate).

***Keywords*—**Fracture Mechanics, Mixed Mode, Arcan Specimen, Finite Element.

I. Introduction

IN recent years the application of composite materials in automotive, aerospace and marine industries have increased so much. The ability of these materials to be designed to suit a particular purpose makes them desirable for many usages. Manufacturing processes and available materials for a specific needs vary in a wide range. [1]

Preventing failure of composite material systems has been an important issue in engineering design. The two types of physical failures that occur in laminated composite structures and interact in complex manner are interalaminar and interlaminar failures. Interalaminar failure is manifest in micro-mechanical components of the lamina such as fiber breakage, matrix cracking, and debonding of the fiber- matrix interface. Interlaminar failure such as delamination refers to debonding of adjacent lamina. The possibility that interalaminar and interlaminar failure occur in structural components is considered a design limit, and establishes restrictions on the usage of full potential of composites. [2]

Due to the lack of through-the-thickness reinforcement, structures made from laminated composite materials and adhesively bonded joints are highly susceptible to failure caused by interfacial crack initiation and growth. The delamination phenomenon in a laminated composite structure may reduce the structural stiffness and strength, redistribute the load in a way that the structural failure is delayed, or may lead to structural collapse. Therefore, delamination is not necessarily the ultimate structural failure, but rather it is the part of the failure process which may ultimately lead to loss of structural integrity [3].

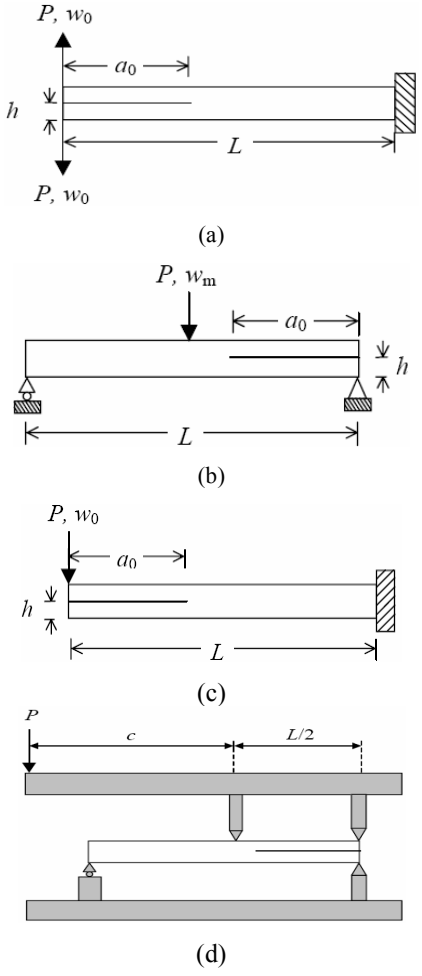

Fig. 1 Most applicable configurations for delamination testing (a) double cantilever beam (DCB) for mode I, (b) end-notch flexure (ENF) and (c) end load split (ELS) for mode II, (d) mixed mode bending (MMB) for mixed mode I&II testing

Authors are with Department of Mechanical Engineering, Sahand University of Technology, Tabriz, Iran (e-mail: mn_au@hotmail.com, choupani@sut.ac.ir).

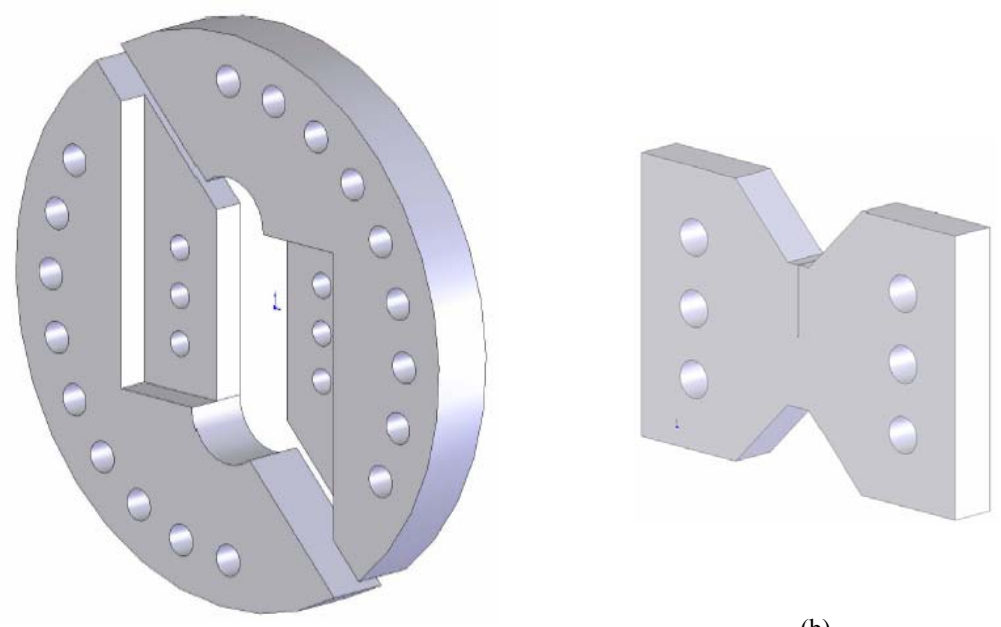

(a) (b)

Fig 2 (a) Arcan apparatus, (b) Arcan specimen

For a given Interlaminar defect, Crack propagation may be accomplished in opening mode (mode-I), shearing mode (mode-II), and tearing mode (mode-III). [4] There are many configuration presented for testing the delamination in mode I, mode II and mixed mode condition in literatures. Double cantilever beam (DCB) method in 1989 by Williams for mode I of fracture, End-Notch Flexure (ENF) method by Carlson in 1986 for mode II of fracture and Mixed Mode Bending (MMB) method by Crews and Reeder for first time in 1988 for mixed mode fracture are used to estimate fracture toughness of different materials (Fig. 1). MMB method is modified and use for calculating the critical interlaminar fracture toughness of AS4/PEEK by Reeder in 1990. [5]-[9]

A new apparatus is presented by Szekrenyes with combining DCB and ENF configurations. The new specimen could be loaded via three point bending machine. The prominences of this specimen are addressed in this paper [10] and [11].

Priel tested the fracture modes of I and II and mixed mode I&II via three points bending apparatus and compared the results such as critical loads and initiation angle with the related criterion. Results show good agreement with some of these analytical results. [12]

Experimental observation indicates that delamination is usually initiated by high interlaminar stresses at or near geometric discontinuities, material discontinuities, material defects, and interalaminar failures, among other stress raisers. Geometric discontinuities include biomaterial systems; material defects include voids; and interalaminar failures include transverse matrix cracks. If free to do so, each ply of a laminate would deform independently of the other plies due to varying fiber orientation and anisotropy of the laminated composite material. Large stresses at the stress raisers boundaries are necessary to preserve compatible deformations, which are primarily responsible for the nucleation of delamination.

Much of numerical investigations presented in literatures lead to excellent results. These methods are more preferable because of their low cost and time consuming.

Finite element models which use 3D SHELL elements demonstrated good accordance with experimental results. Initiation and propagation of delamination studied numerically with using cohesive elements and different constitutive laws lead to excellent results. [13]-[15].

In an experiment done via Brazilian Disk, critical interlaminar fracture toughness for Carbon-Epoxy composite fiber with direction of -45/+45 is calculated. [16]

In another study, the Brazilian disk was used to calculate the critical fracture toughness of carbon-epoxy composite in different loading condition and mixed mode ratios and was demonstrated that fracture toughness of mode II is more sensitive to loading speed rather than mode I fracture toughness. [17]

Arcan specimen for the first time in 1978 was presented for providing plane stress condition in fracture test of mode-I, mode-II and mixed mode condition. This apparatus latter was used for developing COD criterion. The influence of finite geometry and type of material is studied by HalBack numerically and experimentally for two types of Aluminum specimens. The fracture behavior and transformation between mode I and mode II is also investigated in this paper. [18]-[26] In latter experiments conducted with Ayatollahi and Hong, mode II of fracture is studied separately by this configuration.

In this research correction factors of Arcan specimens are calculated via the Arcan apparatus modeling in ABAQUS finite element software and critical interlaminar fracture stress

intensity factor of Carbon-Epoxy cross-ply composite was calculated and also the influence of crack length ratio on stress intensity factors for different loading angles and energy released rate was investigated.

II. Theoretical Backgrounds

The main problem of predicting the failure of composite materials is to characterize the resistance to delamination in terms of interlaminar fracture toughness especially under mixed-mode loading conditions. Linear elastic fracture mechanics has been found a useful tool for investigating of interlaminar cracks in composite materials. It is assumed that the specimens are made of orthotropic linear elastic material with deformability defined by the generalized Hook's law:

$$\begin{pmatrix} \varepsilon_x \\ \varepsilon_y \\ \varepsilon_z \\ \gamma_{yz} \\ \gamma_{xz} \\ \gamma_{xy} \end{pmatrix} = \begin{pmatrix} a_{11} & a_{12} & a_{13} & a_{14} & a_{15} & a_{16} \\ a_{21} & a_{22} & a_{23} & a_{24} & a_{25} & a_{26} \\ a_{31} & a_{32} & a_{33} & a_{34} & a_{35} & a_{36} \\ a_{41} & a_{42} & a_{43} & a_{44} & a_{45} & a_{46} \\ a_{51} & a_{52} & a_{53} & a_{54} & a_{55} & a_{56} \\ a_{61} & a_{62} & a_{63} & a_{64} & a_{65} & a_{66} \end{pmatrix} \quad (1)$$

Where the terms of the nonzero entries of the orthotropic compliance matrix are defined in terms of the following engineering elastic constants:

$$a_{11} = \frac{1}{E_x}, \quad a_{22} = \frac{1}{E_y}, \quad a_{33} = \frac{1}{E_z}, \quad a_{44} = \frac{1}{G_{yz}}$$
$$a_{55} = \frac{1}{G_{xz}}, \quad a_{66} = \frac{1}{G_{xy}}, \quad a_{12} = a_{21} = -\frac{\nu_{xy}}{E_x} = -\frac{\nu_{yx}}{E_y} \quad (2)$$
$$a_{13} = a_{31} = -\frac{\nu_{xz}}{E_x} = -\frac{\nu_{zx}}{E_z}, a_{23} = a_{32} = -\frac{\nu_{yz}}{E_y} = -\frac{\nu_{zy}}{E_z}$$

For a thin plate with its major dimension and principal material axes in the *xy*-plane, the relation between strain and stress is approximated plane stress:

$$\sigma_z = \tau_{yz} = \tau_{xz} = 0 \quad (3)$$

If the stresses according to above equation are substituted into (1), in can be simplified to yield:

$$\begin{pmatrix} \varepsilon_x \\ \varepsilon_y \\ \gamma_{xy} \end{pmatrix} = \begin{pmatrix} a_{11} & a_{12} & a_{13} \\ a_{21} & a_{22} & a_{23} \\ a_{31} & a_{32} & a_{33} \end{pmatrix} \begin{pmatrix} \sigma_x \\ \sigma_y \\ \tau_{xy} \end{pmatrix} \quad (4)$$

Where $\sigma_x, \sigma_y, \tau_{xy}$ and $\varepsilon_x, \varepsilon_y, \gamma_{xy}$ are in-plane stresses and strains. For thick plates, conditions of plane strain are commonly assumed by taking:

$$\varepsilon_z = \gamma_{yz} = \gamma_{xz} = 0 \quad (5)$$

This assumption in combination with Hooke's generalized law leads to

$$\sigma_z = \frac{-(a_{13}\sigma_x + a_{23}\sigma_y + a_{36}\tau_{xy})}{a_{33}} \quad (6)$$

Consequently, is not an independent quantity and may be removed from Hooke's generalized law

$$\begin{pmatrix} \varepsilon_x \\ \varepsilon_y \\ \gamma_{xy} \end{pmatrix} = \begin{pmatrix} b_{11} & b_{12} & b_{13} \\ b_{21} & b_{22} & b_{23} \\ b_{31} & b_{32} & b_{33} \end{pmatrix} \begin{pmatrix} \sigma_x \\ \sigma_y \\ \tau_{xy} \end{pmatrix} \quad (7)$$

Where the terms of the constants b_{ij} are defined in terms of the following nonzero entries a_{ij} of the orthotropic compliance matrix:

$$b_{ij} = a_{ij} - \frac{a_{i3}a_{j3}}{a_{33}} \ldots . (i, j = 1, 2, 4, 5, 6) \quad (8)$$

For the case in which the *xy*-system coincides with the principal material axes:

$$a_{16} = a_{26} = a_{36} = a_{45} = b_{16} = b_{26} = 0$$
$$b_{12} = \frac{a_{12}a_{33} - a_{13}a_{23}}{a_{33}} \qquad b_{11} = \frac{a_{11}a_{33} - a_{13}^2}{a_{33}}$$
$$b_{22} = \frac{a_{22}a_{33} - a_{23}^2}{a_{33}} \qquad b_{66} = \frac{a_{66}a_{33} - a_{36}^2}{a_{33}} \quad (9)$$

For many composite crack growth is self-similar because of delamination and this leads to partition G value into mode-I and mode-II. The energy release rates for orthotropic material with the crack line parallel to the principal orthotropic direction which coincides with the fiber orientation can be calculated from the following relationships:

$$G_I = \frac{K_I^2}{E_I} \qquad G_{II} = \frac{K_{II}^2}{E_{II}} \quad (10)$$

Where E_I and E_{II} are effective module, and K_I and K_{II} are mode-I and mode-II stress intensity factors, respectively. If the crack plane coincides with the direction of minimum crack resistance in interlaminar problems, the direction of crack propagation is collinear with the original crack and the computed values of G_I, G_{II} and $G_T=G_I + G_{II}$ are physically meaningful. It is assumed that the specimens are orthotropic linear elastic material and effective module E_I and E_{II} are defined as

$$E_{II} = \sqrt{\frac{2}{a_{11}a_{22}}} \frac{1}{\sqrt{\sqrt{\frac{a_{22}}{a_{11}}} + \frac{2a_{12}+a_{66}}{2a_{11}}}} \quad (11)$$

$$E_{II} = \frac{\sqrt{2}}{a_{11}} \frac{1}{\sqrt{\sqrt{\frac{a_{22}}{a_{11}}} + \frac{2a_{12}+a_{66}}{2a_{11}}}} \quad (12)$$

For plane strain condition and

$$E_{I} = \sqrt{\frac{2}{b_{11}b_{22}}} \frac{1}{\sqrt{\sqrt{\frac{b_{22}}{b_{11}}} + \frac{2ab_{12}+b_{66}}{2b_{11}}}} \quad (13)$$

$$E_{II} = \frac{\sqrt{2}}{b_{11}} \frac{1}{\sqrt{\sqrt{\frac{b_{22}}{b_{11}}} + \frac{2b_{12}+b_{66}}{2b_{11}}}} \quad (14)$$

for plane stress condition. [27]

The purpose of fracture toughness testing is to determine the value of the critical stress intensity factor. This material property is used to characterize the resistance to fracture in the design of structural members. The stress intensity factors ahead of crack tip for a modified version of Arcan specimen were calculated by using the following equations:

$$K_I = \frac{P_C\sqrt{\pi a}}{wt} f_1(\frac{a}{w}) \quad (15)$$

$$K_{II} = \frac{P_C\sqrt{\pi a}}{wt} f_2(\frac{a}{w}) \quad (16)$$

where P_C in critical load at fracture, α is loading angle, w is specimen length, t is the specimen thickness and a is crack length. In turn K_I and K_{II} are obtained using geometrical factors $f_1(a/w)$ and $f_2(a/w)$, respectively.

III. Finite Element Modeling

A. Virtual Crack Closure Method

The J-integral is widely accepted as a fracture mechanics parameter for both linear and nonlinear material response. It is related to the energy release associated with crack growth and is a measure of the intensity of deformation at notch or crack tip, especially for nonlinear materials. If the material response is linear, it can be related to the stress intensity factors. Because of the importance of the J-integral in the assessment of flaws, its accurate numerical evaluation is vital to the practical application of fracture mechanics in design calculations. ABAQUS provides a procedure for such evaluations of the J-integral, based on the virtual crack extension/domain integral methods. The method is particularly attractive because it is simple to use, adds little to the cost of the analysis, and provides excellent accuracy, even with rather coarse meshes.

In the context of quasi-static analysis the J-integral is defined in two dimensions as

$$j = Lim_{\Gamma\to 0}\int_{\Gamma} n.H.qd\Gamma \quad (17)$$

Where is contour beginning on the bottom crack surface and ending on the top surface, as shown in Fig. 3, the limit $\Gamma \to 0$ indicates that shrinks onto the crack tip; **q** is a unit vector in the virtual crack extension direction; and **n** is the outward normal to **H** is given by

$$H = QI - \sigma.\frac{\partial u}{\partial x} \quad (18)$$

For elastic material behavior W is the elastic strain energy; for elastic-plastic or elastic-viscoplastic material behavior W is defined as the elastic strain energy plus the plastic dissipation, thus representing the strain energy in an "equivalent elastic material." this implies that the J-integral calculation is suitable only for monotonic loading of elastic-plastic materials.

B. Stress Intensity Factors

The stress intensity factors K_I, K_{II} and K_{III} plays an important role in linear elastic fracture mechanics. They characterize the influence of the of the load or deformation on the magnitude of crack tip stress and strain fields and measure the propensity of crack propagation or the crack driving forces. Furthermore, the stress intensity can be related to the energy release rate (the J-integral) for a linear elastic material through

$$J = \frac{1}{8\pi} K^T.B^{-1}.K \quad (19)$$

where $K = \begin{bmatrix} K_I & K_{II} & K_{III} \end{bmatrix}^T$ and B is called the pre-logarithmic energy factor matrix.

In order to calculate stress intensity factors, interaction integral method is commonly used. In general, the J-integral for a given problem can be written as

$$J = \frac{1}{8\pi}[K_I B_{11}^{-1} K_I + K_I B_{12}^{-1} K_{II} + K_I B_{13}^{-1} K_{III} + (Terms\ \ not\ \ involving\ K_I)] \quad (20)$$

where *I*, *II*, *III* correspond to 1, 2, 3 when indicating the components of *B*. We define the J-integral for an auxiliary, pure mode I, crack- tip field with stress intensity factor k_I, as

$$J_{aux}^{I} = \frac{1}{8\pi} k_I.B_{11}^{-1}.k_I \quad (21)$$

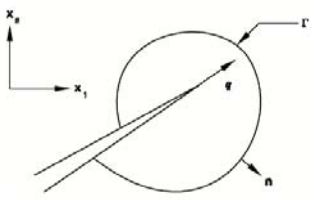

Fig. 3 Contour for calculating J-integral

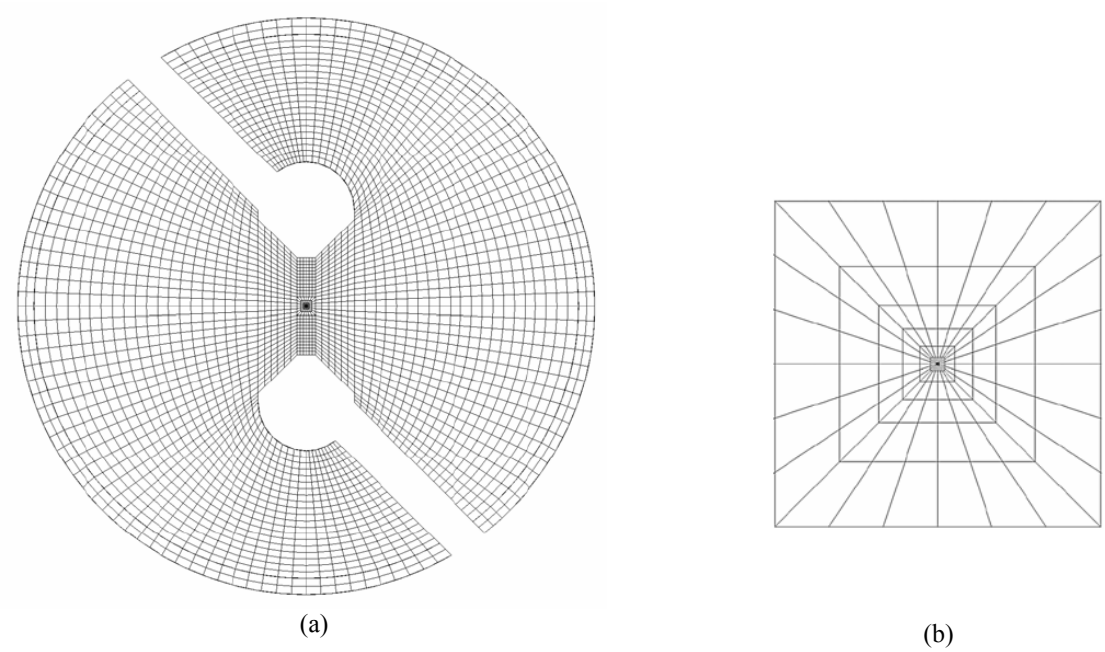

(a) (b)

Fig 4 (a) finite element mesh pattern, (b) fin mesh around the crack tip

Superposing the auxiliary field onto the actual field yields

$$J_{tot}^{I} = \frac{1}{8\pi}[(K_I + k_I)B_{11}^{-1}(K_I + k_I) + 2(K_I + k_I)B_{12}^{-1}K_I + 2(K_I + k_I)B_{13}^{-1}K_{III} + (\textit{Terms not involving } K_I \textit{ or } k_I)] \quad (22)$$

Since the terms not involving K_I or k_I in J_{tot}^{I} are equal, the interaction integral can be defined as

$$J_{\text{int}}^{I} = J_{tot}^{I} - J - J_{aux}^{I} = \frac{k_I}{4\pi}(B_{11}^{-1}K_I + B_{12}^{-1}K_{II}BK + B_{13}^{-1}K_{III}) \quad (23)$$

If the calculations are repeated for mode *II* and mode *III*, a linear system of equation results:

$$J_{\text{int}}^{a} = \frac{k_\alpha}{4\pi}B_{\alpha\beta}^{-1}K_\beta \quad (24)$$

If the k_α are assigned unit values, the solution of the above equation to

$$K = 4\pi B.J_{\text{int}} \quad (25)$$

where $J_{\text{int}} = [J_{\text{int}}^{I}, J_{\text{int}}^{II}, J_{\text{int}}^{III}]^T$ .the calculation of this integral is discussed next.

Based on the definition of the J-integral, the interaction integrals J_{int}^{α} can be expressed as

$$J_{\text{int}}^{\alpha} = Lim_{\Gamma\to 0}\int_{\Gamma} n.M^{\alpha}.qd\Gamma \quad (26)$$

with M^{α} give as

$$M^{\alpha} = \sigma : \varepsilon_{aux}^{\alpha} I - \sigma.\left(\frac{\partial u}{\partial x}\right)_{aux}^{\alpha} - \sigma_{aux}^{\alpha}.\frac{\partial u}{\partial x} \quad (27)$$

The subscript *aux* represent three auxiliary pure Mode I, Mode II, and Mode III crack-tip fields for $\alpha = I, II, III$, respectively. Γ is a contour that lies in the normal plane at position *s* along the crack front, beginning on the bottom crack surface and ending on the top surface (Fig 3). The limit $\Gamma \to 0$ indicates that shrinks onto the crack tip.

To evaluate these integrals, ABAQUS defines the domain in terms of rings of element surrounding the crack tip. Different "contours" (domains) are created. The first contour consists of those elements directly connected to crack tip nodes. The next contour consists of the ring of elements share nodes with the elements in the first contour as well as the elements in the first contour. Each subsequent contour is defined by adding the next ring of element that share nodes with the elements in the previous contour.

The numerical analysis were performed with ABAQUS finite element software under a constant load of 1000 N. the entire apparatus was modeled using eight node collapsed quadrilateral elements and the mesh was refined around crack tip, so that the smallest element size found in the crack tip elements was approximately o.25 mm. al linear elastic finite element analysis was performed under a plain strain condition using $1/\sqrt{r}$ stress field singularity. To obtain a $1/\sqrt{r}$ singularity term of the crack tip stress field, the elements around the crack tip were focused on the crack tip and the mid-side nodes were moved to a quarter point of each element side. [28]-[30]

IV. Results and Discussion

A. Mixed-Mode Interlaminar Fracture Specimen Calibration

In order to determine fracture toughness from (15) and (16) the correction factor of $f_1(a/w)$ and $f_2(a/w)$ must be calculated through finite element modeling of specimen.

The geometrical factor or non-dimensional stress intensity factor for Carbon-Epoxy composite is shown in Fig. 5, in which (*a/w*) ratio varies between 0.1 and 0.7 with 0.1 intervals and also a fifth order polynomial was fitted to the results. Here *a/w* is the crack length ratio, where *a* is the crack length and *w* is the specimen length and a was chosen to be 15mm and w was 30mm respectively.

$$f_1(a/w) = 533.1(a/w)^5 - 965.4(a/w)^4 + 681.1(a/w)^3 - 218.0(a/w)^2 + 33.98(a/w) - 1.146 \quad (28)$$

$$f_2(a/w) = 21.96(a/w)^5 - 44.89(a/w)^4 + 39.22(a/w)^3 - 17.39(a/w)^2 + 5.963(a/w) - 0.18 \quad (29)$$

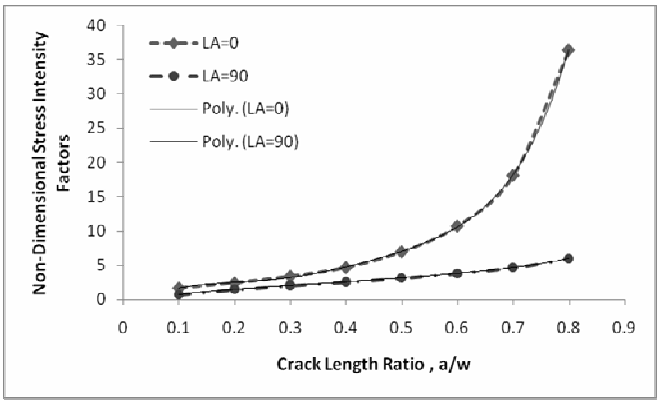

Fig 5 Non-dimensional stress intensity factors vs. crack length of Carbon-Epoxy composite

The relationship between non-dimensional stress intensity factors and Loading angle is demonstrated in Fig. 6, this figure shows which mode is dominant in fracture process. It can be seen that for loading angles less than 45˚, mode-I is dominant and after that mode-II is dominant and when mode-II stress intensity factor increases mode-I stress intensity factor decreases.

Change of strain energy versus change of loading angle is demonstrated in Fig. 7, increase of loading angle from 0 to 90 leads to a vast reduction of strain energy and this causes a great increase of fracture resistance of structure, Also decrease of crack length ratio leads to a same effect on fracture resistance.

Figs. 8 and 9 shows the effect of increase of loading angle and crack length ratio on stress intensity factors of mode-I and mode-II. Increase of loading angle increases the stress intensity factors of mode-II and decreases mode-II stress intensity factor, also, increase of crack length according to the following relationships, increases the normal stress acting at crack tip and also stress intensity factors. [31]

$$\sigma_{yy} = \sigma_a \left\{ 1 + \sqrt{\frac{a}{r}} \left[2\left(\sqrt{\frac{E_{yy}}{E_{xx}}} - \nu_{yx} \right) + \frac{E_{yy}}{G_{xy}} \right]^{1/2} \right\} \quad (30)$$

$$K_I = \lim_{r \to 0} \sigma_{yy} \sqrt{2\pi . r} \quad (31)$$

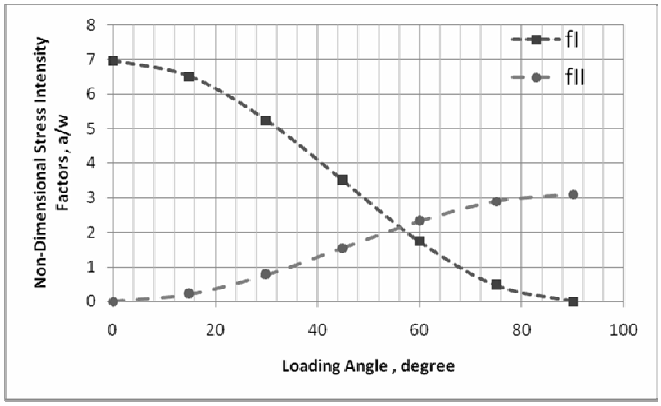

Fig. 6 Non-dimensional stress intensity factors vs. loading angle

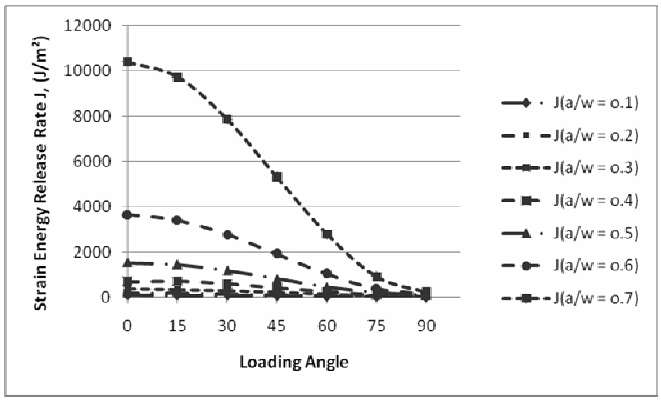

Fig. 7 Strain energy release rate vs. change of loading angle

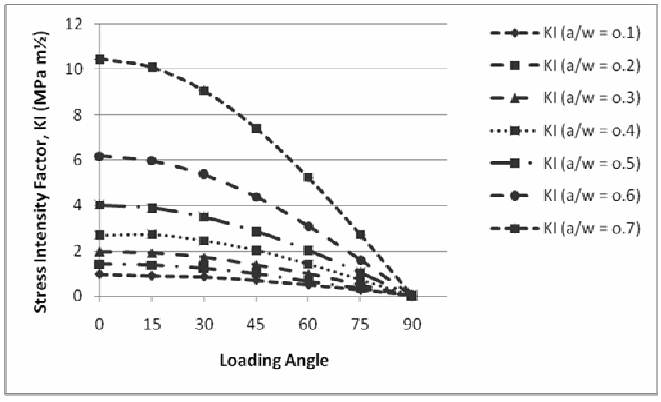

Fig 8 Mode-I stress intensity factor vs. loading angle for different crack length ratio

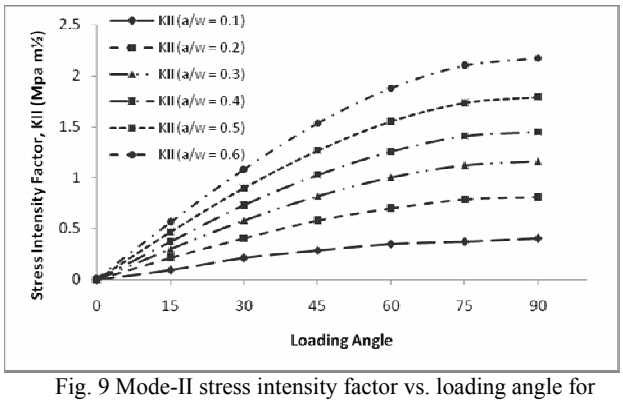

Fig. 9 Mode-II stress intensity factor vs. loading angle for different crack length ratio

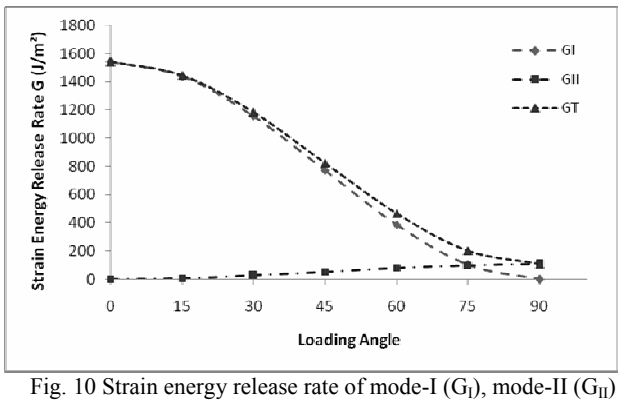

Fig. 10 Strain energy release rate of mode-I (G_I), mode-II (G_{II}) and total strain energy (G_T) vs. loading angle

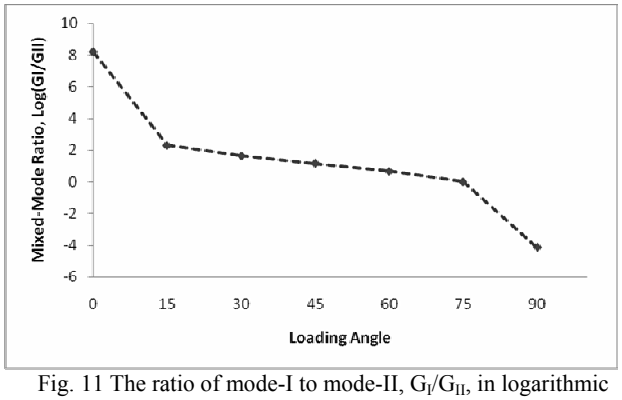

Fig. 11 The ratio of mode-I to mode-II, G_I/G_{II}, in logarithmic scale vs. loading angle

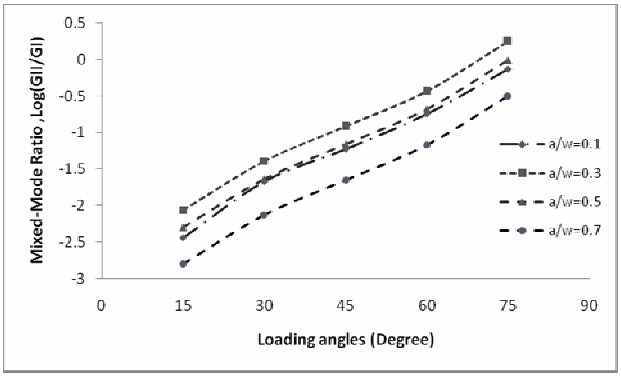

Fig. 12 Mixed-mode ratio, Log (G_{II}/G_I) vs. loading angles for different crack length ratios

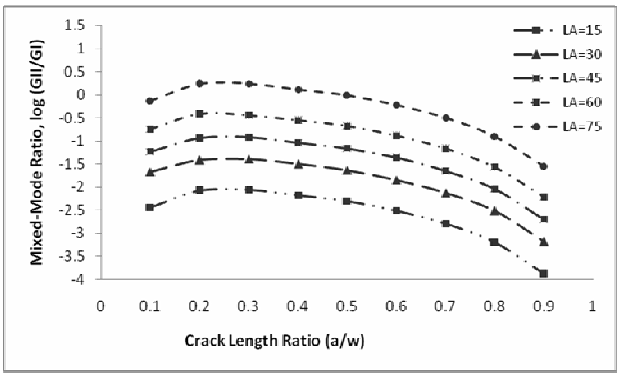

Fig 13 Mixed-mode ratio vs. crack length ratio for different loading angles

B. *Effect of Mixed-Mode Ratio on Interlaminar Fracture*

The strain energy release rates were calculated using (10) and the relationship between strain energy release rate and mixed-mode ratio is showed in Fig. 11. For loading angles near pure mode-I or less than 1, G_I is very larger than G_{II} and in opposite for loading angles greater then 75, G_{II} is dominant. Also can be seed that a wide range of mixed-mode ratio is available through Arcan specimen.

In Fig. 10 the strain energy released rate for pure mode-I and pure mode-II and also total release energy is demonstrated. These quantities are calculated through (10) to (14) for a constant load. This diagram also confirms the results of previous diagrams. For $\alpha \geq 7$ mode-II fracture becomes dominant. The total strain energy release rate under mixed-mode loading condition decreases with the loading angle. Therefore, the increase of the mode-II loading contribution leads to a reduction in the total strain energy release rate.

Variations of mixed-mode ratio due to changes of the crack length ratio for different loading angles and variation of it due to change of loading angle for different crack length ratio is demonstrated in Figs. 12 and 13. Loading angles of 0 and 90 is not involved in the figures because in this loading angle the ratio of G_{II}/G_I became infinity or zero. First in Fig. 12 can be seen that increase of loading angle results in increase of energy release rate and thus increase of mixed mode ratio. The effect of changes of crack length can be observed in Fig. 13. In this figure increase of crack length except in one case in other cases causes a light reduction in mixed mode ratio, this means that increasing of crack length leads to increase of influence of mode-I in fracture process by increasing the energy released rate of G_I in other words, growth of crack length reduce the mode-I material resistance more than mode-II resistance and body tendency to mode-I fracture increases.

V. Conclusion

In this paper the mixed-mode interlaminar fracture behavior of Carbon-Epoxy composite specimens was investigated based on numerical analyses. The behavior of Carbon-Epoxy laminated composite is studied numerically by modeling of Arcan specimen in ABAQUS finite element software. The modeling was fulfilled in the way that loading can be carry out in different loading angles and also analyses is repeated for wide range of crack length ratio between 0.1 to 0.9. The finite element results indicate that for loading angles close to pure mode-II loading, a high ratio of mode-II to mode-I fracture is dominant and there is an opposite trend for loading angles close to pure mode-I loading. It confirms that by varying the loading angle of Arcan specimen pure mode-I, pure mode-II and a wide range of mixed-mode loading conditions can be created and tested. Also, numerical results confirm that the increase of the mode-II loading contribution leads to an increase of fracture resistance in the CF/PEI composite (i.e., a reduction in the total strain energy release rate) and the increase of the crack length leads to a reduction of interlaminar fracture resistance in the CF/PEI composite (i.e., an increase in the total interlaminar strain energy release rate).

References

[1] B. S. Majumdar and D. Hunston. "Continuous Parallel Fiber composite fracture." Encyclopedia of materials: science and technology. Pp 1618-1629.2001.

[2] James R. Reeder. K. Song, P. Chunchu, D. R. Ambur, "Postbukling and growth of delamination in composite plates subjected to axial compression." AIAA journal, 2002.

[3] Carlsson LA, Gillespie JW, Pipes RB. "On the analysis and design of end notched flexure (ENF) specimen for measuring mode II fracture toughness." Composite science and technology 1986.

[4] ABAQUS user's manual, version 6.5. Pawtucket, USA: Hibbit, Karlsson and Sorensen, HKS Inc; 2004.

[5] JG. Williams. "End correction for orthotropic DCB Specimen." Comp science and technology, 1989.

[6] John H. Crews, Jr. and James R. Reeder. "A mixed mode bending apparatus for delamination testing." NASA technical memorandum 100662, August 1988.

[7] James R. Reeder and John R. Crews. "Mixed Mode Bending Method for Delamination Testing." Published in AIAA Journal, vol 28, 1990, pages 1270-1276.

[8] James R. Reeder. "Refinements of the mixed mode bending test for delamination toughness." NASA Langley research center, Hampton, VA, 23681-2199, 1990.

[9] James R. Reeder. "3d mixed mode delamination fracture criteria-an experimentalist perspective." NASA Langley research center,M/S 188E, Hampton VA 23681-2199,USA.

[10] Andras Szekrenyes. "Delamination fracture analysis in the GI-GII plane using prestressed transparent composite beams." International journal of solids and structures 44(2007) 3359-3378.

[11] Andras Szekrenyes. "Prestressed fracture specimen for delamination testing of composites." International journal of fracture (2006) 139: 213-237.

[12] E. Priel, A. bussiba, I. Gilad, Z. Yosibash. "Mixed mode failure criteria for brittle elastic V-notched structures." International journal of fracture (2007) 144: 247-265.

[13] Ronald Krueger. "A shell/3D modeling technique for delamination in composite laminates. In proceedings of the American society for composites," 14th technical conference, technomic publishing, 1999.

[14] Ronald Krueger, P. J. Minguet, T. K. O'Brien. "Implementation of interlaminar fracture mechanics in design: an overview.", Presented at 14th international conference on composite materials (ICCM-14), San Diego, July 14-18,2003.

[15] R. Krueger, D. Goetze. "Influence of finite element software on energy release rates computed using the virtual crack closure technique." NASA/CR-2006-214523, NIA Report No. 2006-06.

[16] C. Liu, Y. Huang, M.L. Lovato, M.G. Stout. "Measurement of the fracture toughness of fiber reinforced composite using the Brazilian geometry." International journal of fracture 87: 241-263.1997.

[17] L. Banks-Sills, Y. Freed, R. Eliasi, V.Fourman. "Fracture toughness of the +45/-45 interface of laminate composite." International journal of fracture (2006) 141: 195-210.

[18] P. Davies et al. Standard test method for delamination resistance of composite materials: current status, applied composite materials 5: 345-364, 1998.

[19] F. F. Dharmawan, G. Simpson, I. Herszberg, S. John. "Mixed mode fracture toughness of GFRP composites." Composite Structures,2006

[20] M. Arcan, Z. hashin, A. voloshin, "A method to produce uniform plane stress state with application to fiber-reinforced materials," Experimental mechanics. 1978.

[21] M.A. Sutton, W. Zhao, M.L. Boone, A.P.Reynolds, D.S. Dawicke, "Prediction of crack growth direction for mode I/II loading using small-scale yielding and void initiation/growth concepts." International Journal of Fracture, 83, 1997.

[22] M.R. Ayatollahi, R. Hashemi. "Mixed mode Fracture in an inclined center crack repaired by composite patching." Composite structure, 81, 264-273, 2007.

[23] M.R. Ayatollahi, D.J. Smith and M.J. Pavier."Crack-tip Constraint in mode II deformation." International Journal of Fracture, 113, 2002.

[24] S.C. Hung and K.M. Liechti. "An evaluation of the Arcan specimen for determining the shear module of fiber reinforced composites." Experimental mechanics, volume 37, no. 4, December 1997.

[25] N. Hallback. "The influence of finite geometry and material properties on mixed mode I/II fracture of aluminum." International journal of fracture 87: 151-188, 1997.

[26] Naghdali Choupani. "Experimental and numerical investigation of the mixed mode delamination in Arcan laminated specimens." Material science and technology, volume 478: 229-242,2008.

[27] M.W. Hyer. "Stress analysis of fiber reinforced composite materials." McGrow-Hill.1997.

[28] S. Courtin, "Advantages of the J- integral approach for calculating stress intensity factors when using the commercial finite element software ABAQUS," Engineering Fracture Mechanics,2005.

[29] J.M.Q. Oliveira, A. Haddi, A. Seddak, A. lavie. "Numerical analysis of the MMB test for mixed mode I/II wood fracture," composite science and technology 67 (2007).

[30] ABAQUS user's manual, version 6.5. Pawtucket, USA: Hibbit, Karlsson and Sorensen, HKS Inc; 2004.

[31] A. T. Zehnder. "Lecture on fracture mechanics." Cornell University.2007.